



Research article

Bio-based composites of sago starch and natural rubber reinforced with nanoclays

Jareerat Ruamcharoen^{1*}, Ruzana Munlee¹, Lapporn Vayachuta², Polphat Ruamcharoen³

¹Faculty of Science and Technology, Prince of Songkla University, Muang, 94000 Pattani, Thailand

²National Nanotechnology Center (NANOTEC), National Science and Technology Development Agency (NSTDA), Khlong Luang, 12120 Pathum Thani, Thailand

³Rubber and Polymer Technology Program, Faculty of Science and Technology, Songkhla Rajabhat University, Muang, 90000 Songkhla, Thailand

Received 6 May 2023; accepted in revised form 12 July 2023

Abstract. Sago starch (SS) was blended with natural rubber (NR) using nanoclays, namely montmorillonite (MMT), kaolinite (KAO), and kaolinite modified by dimethyl sulfoxide (KAO-D) to enhance its physical and mechanical properties. Each nanoclay was incorporated at 2, 4, 6, and 8 wt%, respectively. The SS80NR20 (80 wt% of sago starch and 20 wt% of natural rubber) biocomposites were characterized by solubility of water, water vapor transmission, mechanical and thermal properties. The constituent interaction and morphology of the SS80NR20 biocomposites were also presented by using X-ray diffraction (XRD) technique and scanning electron microscope (SEM). The findings demonstrated that the inclusion of clays significantly improved both the water resistance and tensile properties when compared to the SS80NR20 blend. In the SS80NR20 biocomposites, MMT at 6 wt% exhibited the lowest moisture content, solubility in water, and water vapor transmission. As the amount of nanoclay in the biocomposites increased, their tensile strength dramatically increased whilst their strain at break had a tendency to diminish. Strong interaction by establishing the intercalated structure of MMT, and KAO within SS80NR20 biocomposites were attributed to both physical and mechanical properties, while the weak interaction at the interface of SS and NR was attributed to KAO-D.

Keywords: sago starch, clay, natural rubber, biocomposites

1. Introduction

Utilizing natural resources effectively and creating innovative eco-friendly technology are the cornerstones of the sustainable development concept. As the environmental crisis and petroleum depletion grow more seriously and in response to the Sustainable Development Goals (SDGs) policy, chemicals and materials made from natural and recycled resources have attracted a lot of attention [1]. One of several strategies for minimizing the negative impact of petroleum-based plastic materials on the environment is the use of biodegradable materials for replacement of synthetic materials [2–7]. Due to its

naturally renewable nature, low cost, and wide availability, starch is one of the most prominent raw materials used to produce biodegradable materials. There have been many research studies on the development of starch-based films made from different starches *i.e.*, potato, and cassava starch including high-amylose starch [8–14], but there has been relatively few research on sago starch film formation and its application [15–17].

Sago starch is extracted from sago palm (*Metroxylon* spp.) which is distributed throughout Southeast Asia. It has distinctive features, nevertheless, some of its physicochemical characteristics are extremely

*Corresponding author, e-mail: jareerat.su@psu.ac.th

© BME-PT

comparable to those of typical starches like potato and cassava [17, 18]. The features of the hot paste and the temperatures are also extremely like potato starch, whereas the amylose amount and the temperatures of gelatinization are very similar to maize starches [18]. The intriguing thing about sago starch is that it contains more fiber, phenolic compounds, waxes, and lipids than other starches, which helps the starch film swell in water relatively slowly [17]. Therefore, it is possible that sago starch (SS) can be developed as a biopolymer film for packaging. Unfortunately, numerous limitations make sago starch-based polymers show poor inherent properties, such as relatively low mechanical properties, poor water resistance, and barrier properties [13–17].

To enhance their mechanical properties and minimize the dependence of their behavior on the presence of water, thermoplastic starches have, on the other hand, been successfully blended with other appropriate polymers to generate the interesting renewable polymer, associated with starch [19–23]. For instance, the blend of cassava starch (CS) with natural rubber (NR) is based on the different characteristics between CS and NR, resulting blend with distinctive properties different from the initial polymers are expected. NR is an emulsion (latex state) composed primarily of long linear chains of cis-1,4 polyisoprene and trace amounts of mineral salts, phospholipids, and glycoproteins. Chemical compatibility between starch and NR blend, which is currently very poor due to the hydrophobic-hydrophilic antagonistic relationship, is another factor that affects blend performance [19–23].

The mechanical properties of blends of starch and NR produced using conventional methods are considered extremely poor owing to incompatibility and poor water resistance. The apparent immiscibility of hydrophilic starch and hydrophobic NR, however, results in phase-separated blends with poor interfacial characteristics that can be solved by compatibilization [20–23].

Furthermore, gelatinizing starch is an effective method for improving the interfacial interaction between different phases. The addition of the compatibilizer is also generally preferred due to its ability to improve the system's properties. The addition of fillers into a binary polymer which is incompatible has been shown to influence phase morphology caused by the interaction of the blend's individual components with the solid surface. Organoclay has

been used as a reinforcing and compatibilizing filler in polymer blends [22–30]. The extent of the silicate nanolayer dispersion, as well as the clay type and elastomer compatibility, have all been found to have a strong influence on the properties of the compounds. Furthermore, the smaller size of the dispersed phase droplets was obtained. This suggested that the clay could act as a compatibilizer, decreasing the interfacial tension between the two polymer phases [24–28]. However, there are not many studies on NR disperse phase added to the starch in gelatinized form. Hydrophilic starch and hydrophobic NR are inherently incompatible, resulting in phase-separated blends with interfacial properties that can be improved by nanoclay compatibilization [22, 23].

In this research, preliminary experiments have already been performed by varying the ratios between sago starch and natural rubber as follows: 100:0, 95:05, 90:10, 80:20, 70:30 60:40, and 50:50 by weight, respectively. The addition of rubber into the blend was limited by phase separation. The appearance of which also depended on the glycerol content. It was found that the ratio of SS and NR with 80:20 is the ratio in which the minimum content of sago starch begins phase separation of both phases, resulting in a decrease in mechanical properties and water vapor permeability. This also agrees with other reports [19, 21]. Numerous factors, such as the distinctive formulation ratio of SS and NR (80:20), and the incorporation of nanoclays namely montmorillonite, kaolinite, and kaolinite modified with dimethyl sulfoxide as reinforcing agents, could contribute to the originality of the blend. These factors may contribute to improved physical and mechanical properties, such as increased tensile strength, enhanced flexibility, improved tear resistance, or better thermal stability. Regarding the applications, it would be valuable to highlight the potential industries or fields where the SS-NR blend could find utility. For example, it could be relevant in the development of biodegradable packaging materials, eco-friendly adhesives, or biomedical products with enhanced mechanical properties and biocompatibility [15, 17].

Additionally, gelatinizing starch is an effective way to increase the affinity at the interfaces between the different phases. Besides that, it is always desirable to enhance the properties of the blends through the addition of the compatibilizer. This research studied the effects of different types and amounts of nanoclays on sago starch blended with NR prepared

via a solution blending and casting process. The nanoclays were used in various amounts, and their effects on the structure and properties of the bio-based composites were characterized. The goals of this study were to identify the optimal nanoclay contents that provided the greatest properties and to elucidate the relationship between the structures and properties of various biocomposite film formulations.

2. Experimental

2.1. Materials

Sago starch was extracted from the starch granules found in the sago palm (*Metroxylon* spp.) in the southern part of Thailand. It comprises 23.9 wt% of amylose, 0.19 wt% of protein, 0.04 wt% of lipid, 0.13 wt% of lignin, and 0.54 wt% of acid detergent fiber. High ammonia natural rubber latex with 60% dry rubber content was purchased from Chana Latex company. Glycerol used as a plasticizer in starch was supplied from Ajax Finechem Pty Ltd. (Australia). Montmorillonite (MMT) and kaolinite (KAO) clays were purchased by Amarin Ceramics Co., Ltd. (Nonthaburi, Thailand). 100 g of clays (MMT and KAO) was dispersed in distilled water with a homogenizer at 15000 rpm for 1 h. The MMT and KAO clays were cleaned by soaking in a concentrated HCl solution overnight to remove the iron oxide. After that, white clay was collected by filtration and dried in an oven at 60 °C. Then it was kept in a container that was sealed. The kaolinite clay was modified by dimethyl sulfoxide to enhance the d-spacing of silicate layers of kaolinite [16].

2.2. Bio-based composite preparation

100 ml of de-ionized water and sago starch (80 wt% of starch) were dispersed in a beaker, and the mixture was continuously agitated at 80 °C to produce a homogenous solution and ensure even dispersion of all ingredients. After that, glycerol (30 wt% of starch) as a plasticizer was added to the gelatinized starch solution, and NR latex (20 wt% of dry rubber) was also mixed. Three types of nanoclay *i.e.* montmorillonite, kaolinite, and KAO modified with dimethyl sulfoxide (KAO-D) with various amounts of 2, 4, 6, and 8 wt% of starch were added and stirred for 1 h. The SS80NR20 blended solution was then poured onto the polyethylene plates and allowed to dry for 48 h at 50 °C. The thickness of the biocomposite film was then measured in five replications with a micrometer. All abbreviations of the formula used are

shown as follows: SS80NR20 represents the 80 wt% of sago starch and 20 wt% of natural rubber while SS80NR20MMT, SS80NR20KAO, and SS80NR20KAO-D represent 80 wt% of sago starch, 20 wt% of natural rubber containing MMT, KAO and KAO-D, respectively.

2.3. Bio-based composites characterization

2.3.1. Moisture test

The moisture content of SS80NR20 biocomposite films was determined according to ASTM D789 with some modifications. Five samples with 2.0×2.0 cm were weighed to gain the initial weight (W_0). Then, bio-based composite samples were dried in an oven at 110 °C and weighed every hour until constant weight (W_f). The percentage moisture content was given by Equation (1):

$$\text{Moisture content [\%]} = \frac{W_0 - W_f}{W_0} \cdot 100 \quad (1)$$

2.3.2. Water solubility test

The solubility of SS80NR20 biocomposite specimens was measured to gain the weight lost in the water. Five specimens with 2.0×2.0 cm were weighed as the initial weight (W_1). Then, specimens were immersed in distilled water at room temperature. After 24 h, the specimens were dried in an oven at 50 °C for 24 h and weighed to obtain the final weight (W_2). The percentage of solubility was calculated in the Equation (2):

$$\text{Water solubility [\%]} = \frac{W_1 - W_2}{W_1} \cdot 100 \quad (2)$$

2.3.3. Water vapor transmission test

Testing for water vapor transmission (WVT) was done in line with ASTM E96-80 (ASTM 1998). The top of the container was then tightly sealed with a piece of SS80NR20 biocomposite film. The biocomposite film was measured for thickness and diameter and placed in a 75% humidity chamber. The weight change of specimens was measured every 12 h until the sample weight remained constant. The water vapor transmission rate of the sample was calculated from the weight, diameter, and thickness of the film sample as Equation (3):

$$\text{WVT rate} = \frac{W}{A \cdot t} \quad (3)$$

where W is the weight loss of the cup [g], A is the water vapor transmission area [cm²], and t is the time of water vapor transmission [h].

2.3.4. Tensile measurement

Tensile testing was performed in accordance with ASTM 638. The modulus, tensile strength, and elongation at break of SS80NR20 biocomposite films were measured using a universal tensile testing machine (H10KS Hounsfield Test, Tinius Olsen Ltd., United Kingdom) with a 500 N load cell in tensile mode. For each formulation, at least 7 samples with rectangular samples (100×12×~0.25 mm) were clamped between the grips (30 mm initial distance), and tested with a speed of 50 mm/min. The stress and strain were recorded during the test.

2.3.5. X-ray diffraction measurement

Biocomposite specimens were analyzed by X-ray diffractometer (Philips X'Pert MPD, Netherlands) with Cu K_α radiation ($\lambda = 0.154$ nm), operating at 35 kV and 15 mA. The diffraction patterns were recorded from 2.5 to 50° at a scanning rate of 1.5°/min. The d -spacing (d) was calculated according to Bragg's law as shown in Equation (4):

$$2d \sin \theta = n\lambda \quad (4)$$

where n is the order of diffraction, θ is the diffraction angle and λ is the wavelength.

2.3.6. Morphological study

A morphology study was done at the tensile fracture surface of the SS80NR20 biocomposites by using a scanning electron microscope (Quanta 400 model) to observe the NR and nanoclays phase distribution and aggregation. The test specimens were attached to an aluminum mount with double-sided adhesive tape and sputtered with gold (10 nm thickness), on a Polaron SC 515 sputter coater to eliminate electron-charging effects. The samples were examined at an accelerating voltage of 20 kV in the vertical direction. Scanning electron microscope (SEM) micrographs of the biocomposite films were taken at 5000× magnification.

2.3.7. Thermal stability analysis

The thermal decomposition temperature of the SS80NR20 biocomposites was carried out by using

a Perkin Elmer TGA 8000 apparatus. The thermogravimetric analyzer (TGA) was operated at a heating rate of 10 °C/min from 50 to 600 °C under a nitrogen atmosphere.

2.3.8. Dynamic mechanical analysis

Rectangular specimens of the SS80NR20 biocomposites were conditioned for two weeks at 25 °C and 60±5% RH, before being tested using a dual cantilever clamp on a model DMA 1 (Mettler Toledo, Switzerland) dynamic thermo-mechanical analyzer. The measurement was performed at a frequency of 1 Hz and at an amplitude of 2 μm over a temperature range from –100 to 200 °C, at a scanning rate of 5 °C/min. The temperature dependence of storage modulus (E') and $\tan \delta$ was measured in the temperature range from –100 to 200 °C.

3. Results and discussion

3.1. Moisture content and solubility

When natural rubber was blended with sago starch, and clays a lower moisture content compared to pristine sago starch film was obtained as illustrated in Figure 1. It is due to the hydrophobicity of rubber. However, the result of incorporating clays as filler showed a slightly decreased in moisture content. The decrease in the number of water molecules in the internal of SS80NR20 biocomposites due to the insertion of polysaccharide chains of sago starch and rubber molecular chains in the silicate layer, leading to lower water molecule adsorption while kaolinite-added biocomposites absorbed more water molecules. It was due to the less distribution of clay in the biocomposite films. While adding KAO-D presented more decreased moisture content compared

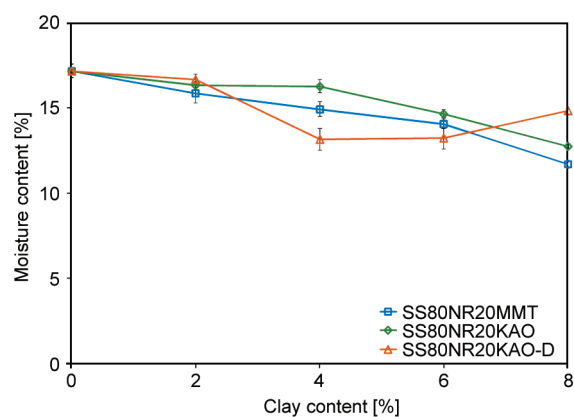


Figure 1. The moisture content of biocomposite films with MMT, KAO, and KAO-D.

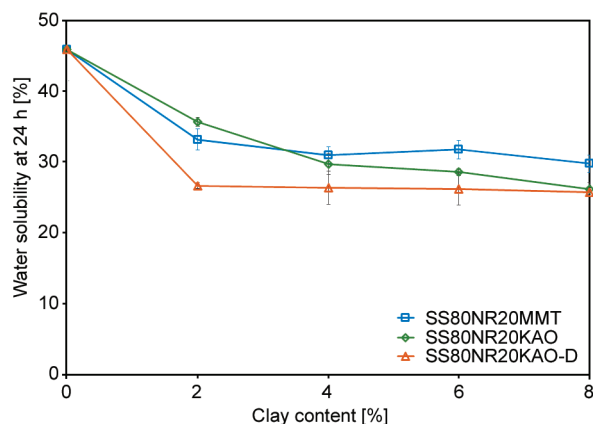


Figure 2. The water solubility of biocomposite films with MMT, KAO, and KAO-D.

with the SS80NR20 blend. This is expected that the silicate layer dispersion of KAO-D in the starch matrix led to diminishing the interaction of water molecules and the polysaccharide chain.

From [Figure 2](#), the escalation of NR to SS increased the water solubility of composites compared to the SS80NR20 blend because of poor compatibility between polar starch and non-polar rubber. However, the addition of clays tended to present that the water solubility of biocomposite films was reduced with the least water-soluble modified kaolinite added biocomposites. It was assumed that the internal structure of KAO-D displayed the separated silicate layers which are facilitated by a better dispersion of the clay in the polymer matrix (exfoliated structure), [16, 24] expecting in good distribution in SS80NR20 biocomposites. This was due to interactions at the interface of nanoclay and polymer whereas SS80NR20 biocomposites blended with MMT exhibited higher water-soluble than those of KAO and KAO-D added on account of the hydroxyl group of the glucose unit of sago starch absorbing the MMT. While MMT clay and rubber are less active, water molecules are easier to insert [8, 23]. Some studies reported a rise in the intermolecular forces between the film's respective components and speculated that hydrogen bonds generated between MMT, and starch chains were stronger than those formed between MMT and starch as well as water [25].

3.2. Water vapor transmission

In assessing SS80NR20 biocomposites for usage in protective coating for food packaging and other applications requiring efficient polymer barriers, the observed dramatic reduction in *WVT* is significant. The water vapor transmission of SS80NR20

biocomposites is exhibited in [Figure 3](#). It was demonstrated that the *WVT* of SS80NR20 biocomposites with the addition of MMT, KAO, and KAO-D was reduced as compared with SS80NR20 blend. In turn, this indicated that nanoclays could improve the *WVT* of SS80NR20 biocomposite films. Surprisingly, when MMT clay was incorporated into SS80NR20 biocomposites, the *WVT* at 24 h was significantly decreased as shown in [Figure 3a](#). *WVT* of the biocomposites with 2 wt% clay decreased by 55% compared to SS80NR20 biocomposites as well as the water vapor transmission slightly decreased with increasing time. A possible explanation for its effect could be that the glucose unit in sago starch was able to form hydrogen bonds with the hydroxyl group of MMT and its stronger structure improve water vapor transmission. This behavior agreed with previous reports [23, 31]. The *WVT* of SS80NR20 biocomposites containing MMT presented the lowest values, indicating that MMT might reduce the number of active sites where water molecules can interact with starch chains, and owing to the presence of dispersed large aspect ratio silicate layers in the polymer matrix as seen in other polymer-layered silicate composites [8, 26]. When kaolinite clay was added to the SS80NR20 biocomposites, it was obviously seen that the water vapor transmission decreased with the addition of 4 and 6 wt% of KAO and KAO-D clay compared to the SS80NR20 biocomposite film as illustrated in [Figures 3b, 3c](#).

It was noteworthy that the water vapor transmission increased with the incorporation of 8 wt% of KAO and KAO-D. This can be explained by the addition of 4 and 6 wt% clay, as well as the good distribution of KAO in the SS80NR20 composites. However, the increment in the amount of kaolinite clay generated the agglomeration of the silicate layer leading to a decrease in water vapor transmission. KAO-D decreased the *WVT* and gave the minimum *WVT* at 6 wt%. This is consistent with the biocomposite film morphology ([Figure 6i–6k](#)) as discussed in Section 3.5. It was found that the clay plates separated to form a silicate layer, the larger the volume resulting in better water vapor transmission. According to the materials' water vapor barrier capacity evaluation, the nanostructure of the SS80NR20 films reinforced with the nanoclay created a more tortuous path for the permeant gas to pass through. The molecules of water vapor diffused through the biocomposite film, following the path of low resistance. Due

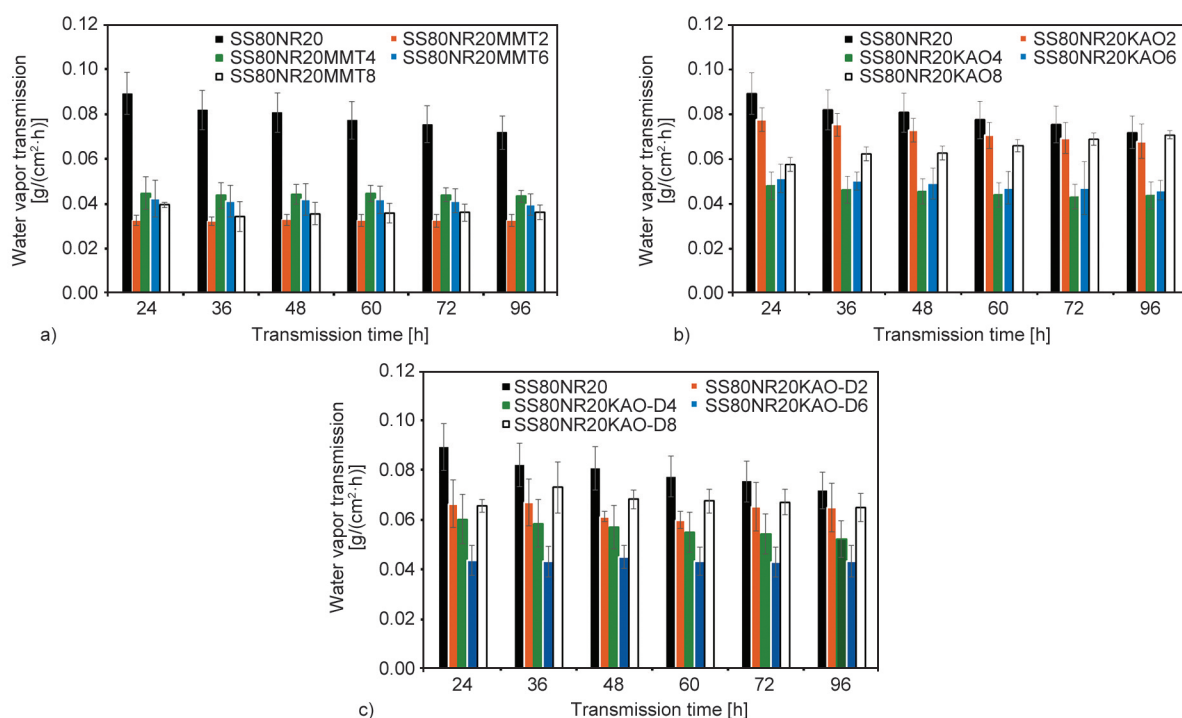


Figure 3. Water vapor transmission of biocomposite films with a) MMT, b) KAO and c) KAO-D.

to the lower specific surface area and the strong polymer/filler interaction of MMT, the *WVT* reduction was slightly greater than that of KAO and KAO-D [16, 23].

3.3. Tensile properties

Regarding the tensile properties of the SS80NR20 biocomposites, the average values of tensile strength, Young’s modulus, and elongation at break are shown in Figure 4. Tensile strength and Young’s modulus values exhibited a significant increment for the SS80NR20 biocomposites with the addition of MMT clay. With the variation of MMT content from 2 to 8 wt% in the SS80NR20 biocomposites, the change in the tensile characteristics can be explained more clearly as shown in Figure 4b. The maximum Young’s modulus and tensile strength found for SS80NR20 biocomposites containing 6 wt% of MMT, were about 3 times higher than that of SS80NR20 blend. As observed in Figure 4b, Young’s modulus for the SS80NR20 film was 23 MPa which was enhanced to 53.2 and 90.5 MPa for 2 and 6 wt% of MMT, respectively. The enhancement of the tensile strength of SS80NR20MMT composites might be caused by the strong surface interaction between MMT and the polymer matrix because of the intercalation of SS and NR in the clay silicate layer. This improvement of the tensile strength is likely to be due to the strong interfacial interaction between MMT and polymer

matrix caused by the intercalation of SS and NR into the clay silicate layers. It is indicated that the distribution of MMT in the self-assembled film is homogeneous [23, 26]. Interestingly, the elongation at break of MMT-filled SS80NR20 biocomposites was also significantly increased. It was possible through the insertion of polysaccharide and rubber chains into the silicate layer of MMT resulting in an intercalated structure as well as a mechanical interlocking between the polymer chain and silicate layer was formed [24, 26]. The tensile properties of KAO-filled SS80NR20 composites slightly increased. An increase in these properties may be due to the reinforcement of kaolinite clay, which was a structurally strong inorganic filler. The tensile strength of SS80NR20 biocomposites containing 4 wt% of kaolinite presented the maximum value when increasing kaolinite content markedly tended to decrease. However, for modulus at 1% strain, the SS80NR20 biocomposites gave the maximum value with 4 wt% of kaolinite. It can be explained that the more kaolinite content up to 6 wt% more coagulation of kaolinite clay was found. This corresponds to the results of X-ray diffraction analysis as shown in Figure 5b. It can be assumed that some polysaccharide and rubber chains can be inserted into the silicate layer of kaolinite acting as intercalated phenomena, while some silicate layers do not alter. This is owing to the very weak interaction between polymer

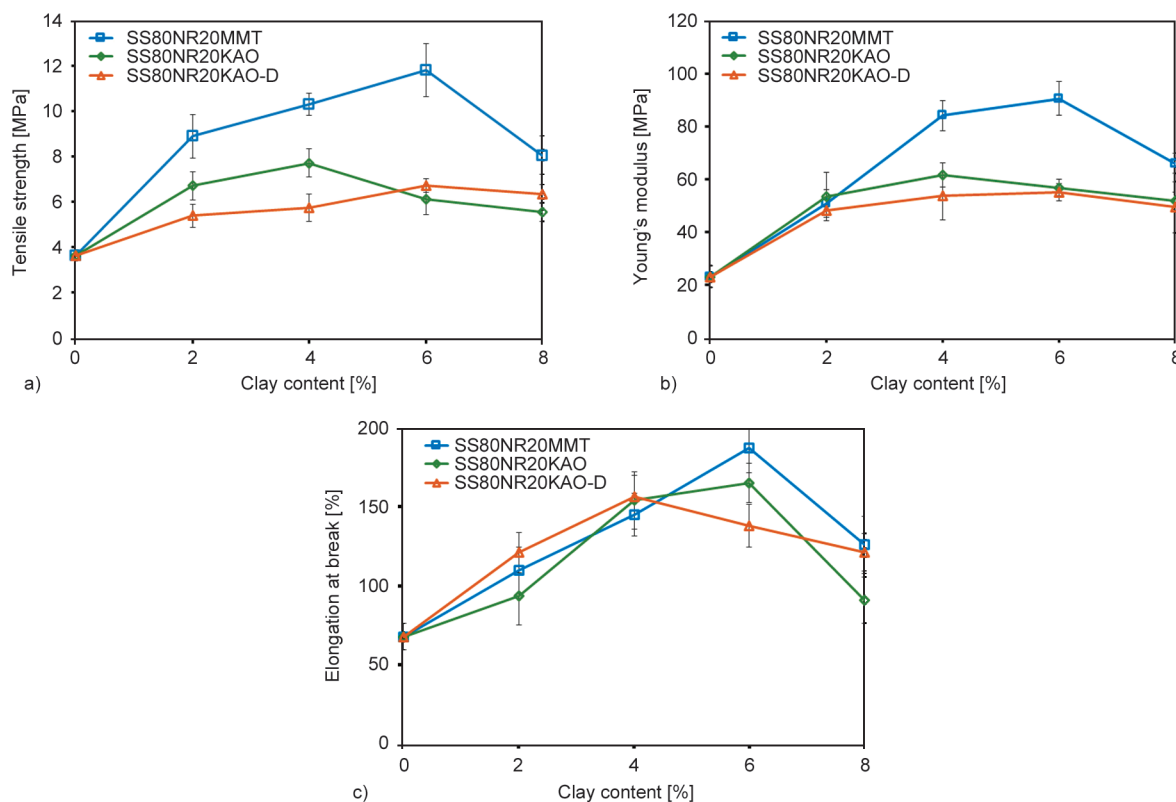


Figure 4. Tensile properties of biocomposite films; a) tensile strength, b) Young's modulus, and c) elongation at break.

and kaolinite clay as the interlayer space of kaolinite is an asymmetrical structure. The asymmetrical structure of $\text{AlO}_2(\text{OH})_4$ octahedral and SiO_4 tetrahedral sheets led to induce strong superposed polarity, in conjunction with hydrogen bonds between the silicon oxide and the alumina surface. As a result, the strong cohesive energy of the kaolinite mineral was reported [13, 16]. By comparing clay effects on the tensile strength and modulus of the SS80NR20 blend with the inclusion of an equal amount of clay (2, 4, 6, and 8 wt%), it was also revealed that the MMT had more reinforcing and compatibilizing effects on SS80NR20 blend. These can be attributed to the stronger interactions of the nanoclay with SS chains in comparison to rubber chains, as evidenced by the SEM results (Figure 6). The results shown in Figure 4c also indicated that the incorporation of the nanoclay into the SS80NR20 blend increased its elongation at break. It is attributed to the compatibilizing role of clay, which promotes interfacial interactions between the SS and NR components. For the SS-rich phase, the reinforcement of the interfacial interactions between the phases due to the presence of the nanoclay in the interface could positively influence their elongation at break. On the other hand,

the localization of the nanoclay in the individual phases, especially the matrix phase, and its interaction with the components decreased the mobility of chains and therefore could negatively affect the elongation at break. Surprisingly, when nanoclay was added to the SS80NR20 system, the elongation at break (*EB*) was markedly increased by the maximum *EB* when 6 wt% nanoclay was added in which the SS80NR20 biocomposites with the addition of MMT having the highest elongation at break of 3 times compared to the SS80NR20 film. The *EB* of 8 wt% of nanoclays in the SS80NR20 blend was significantly reduced. It can be explained that, at higher clay content, the clay particles have a greater tendency to interact and form aggregates. These aggregates can act as stress concentration points, minimizing the overall strength and mechanical properties of the blend. The presence of larger clay aggregates can create voids or weak points within the biocomposites (as seen in Figures 6e, 6h, 6k), leading to a decrease in mechanical performance. Additionally, at higher clay content in the blend, poor dispersion results in weak interfacial bonding between the clay and the polymer matrix, leading to reduce load transfer and lower mechanical properties. It is well known that

the physical and mechanical properties of native SS and NR components are very weak in the absence of compatible or reinforcing agents. Therefore, the physical and mechanical properties of the mixture are also inferior, and this is mainly due to the incompatibility of the two components with each other. The mechanical properties are in accordance with the morphology in Section 3.5.

3.4. Nanoclays dispersion in biocomposites

The X-ray diffraction patterns of SS80NR20 biocomposites are shown in Figure 5. After solution blending, the diffraction character of SS80NR20 biocomposites indicated amorphous sago starch with broad, featureless peaks throughout the whole 2θ scanning range. The X-ray diffraction (XRD) pattern of biocomposites; however, exhibited the MMT-specific peaks with the addition of layered silicates. The MMT presented a diffraction peak crystal plane 001 at $2\theta = 6.92^\circ$ corresponding to the d_{001} of 1.28 nm, whereas the 001 diffraction peaks of MMT in the biocomposites shift toward lower angles, *i.e.*, 6.92° to 5.37° , 5.12° , and 4.87° , which indicated that the interlayer distances increased as shown in Figure 5a. The basal spacings of the MMT were calculated from the XRD peak position using Bragg's equation,

where the d_{001} of MMT in the biocomposites was found to be in the broader range of 1.64 to 1.81 nm. The lateral dimensions of this structural amylose unit were approximately 1.5 nm for each elementary chain, while the *cis*-1,4 polyisoprene structure was approximately 1.5 nm for each chain. The result implied that intercalation of the polysaccharide of SS and rubber chains into the silicate interlayers occurred and expanded the basal spacing. All polymer-clay nanocomposites have XRD patterns that were suggestive of an intercalated structure in which the polysaccharide chains or rubber incorporated between the silicate layers, expanding their gallery height but preserving their layered stacking with interchanging biopolymer/silicate layers as described in a previous report [23, 25].

Characteristic diffraction peaks of the purified KAO can be observed at $2\theta = 8.92^\circ$, 12.37° , and 24.9° . The X-ray diffraction patterns of SS80NR20 biocomposites loading kaolinite clay are shown in Figure 5b. The increase in the kaolinite content in the SS80NR20 biocomposites led the peaks at 8.92° and 12.37° to be more intense, suggesting that the pseudo-crystals were still present. Especially, the intensity of peaks at 8.92° presenting in the SS80NR20 biocomposites revealed the intercalated structure of

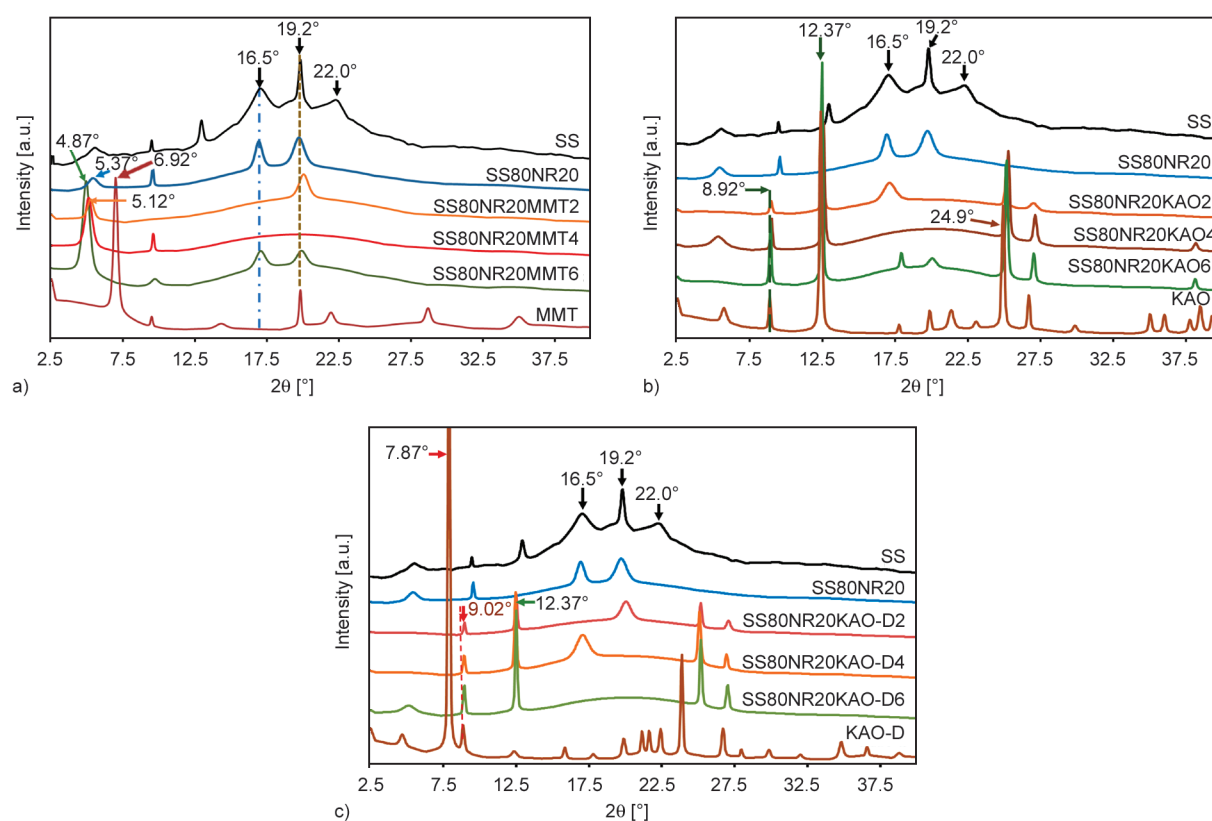


Figure 5. XRD pattern of biocomposite films with a) MMT, b) KAO, and c) KAO-D.

silicate layers by the insertion of some polysaccharide and rubber chains in the silicate layer of kaolinite [13, 16, 23]. Nonetheless, the disappearance of the 7.87° in the dimethyl sulfoxide (DMSO) intercalated kaolinite (KAO-D) in the SS80NR20 biocomposites implied that this component was almost disorganized (Figure 5c). It was found that when added KAO-D, a peak at position 12.37° presented, and more intensity of this peak was observed, while peak 7.87° disappeared. It can be explained that the KAO-D gave more reorganized its silicate layer to form the compact silicate layers in the SS80NR20 biocomposites. This is due to the kaolinite intercalation process explained as a diffusion process, the driving force of which is strong hydrogen bonds formed between the intercalation agent and the hydroxyl group ($-\text{OH}$) of the octahedral sheet. The release of the original crystal interlayer bonds could be a primary or a secondary effect of the intercalation agent. A large dipole moment of organic compound combined with a significant number of intercalated molecules per unit cell favors the formation of an intercalation complex. Therefore, the conventional intercalation agents consisting of both dipole moment and polarizability of glycerol and DMSO with lower values than that of kaolinite are not suitable to intercalate the finer structure of kaolinite. Therefore, in the system there is glycerol, which is more polar than DMSO, thereby reducing the activity rate within the silicate layer, leading to the restoration of the original structure again. As a result, the mechanical properties and water vapor transmission of the SS80NR20 biocomposites adding KAO-D clay were therefore reduced.

3.5. Morphological study

Starch and natural rubber have different properties, and when blended, their stability can be influenced by composition and processing techniques since starch is hygroscopic which can absorb moisture from the surrounding environment. To improve stability, glycerol as a plasticizer [19] and clays were added to the blend to reduce moisture sensitivity [16, 23, 25]. SEM micrographs of the SS80NR20 biocomposites are shown in Figure 6.

The separated phase boundaries of the SS80NR20 blend and clays are seen. The fracture surface of SS and SS80NR20 in Figures 6a, 6b were fairly smooth. The SEM micrographs show rubber particles on the surface of the biocomposite that has undergone tensile fractures, indicating that the compatibility of NR

and SS is less. The surface roughness of the SS80NR20 composite films increased with the nanoclay content. Figure 6c–6k confirmed that the addition of nanoclays with 2, 4, and 6 wt% in the SS80NR20 blend had a significant effect on fracture morphology and behavior. The distinctive phase boundaries of the SS and NR blend can be clearly seen, and they gradually diminished with the addition of 2 and 4 wt% of clays. This suggested that nanoclays may act as interfacial interfaces. It reduced the inter-surface tension by simultaneous dissociation of the NR phase and resulted in a reduction in particle size [23, 27]. It may be inferred that the MMT and KAO clays can help SS and NR become compatible with each other. However, some agglomeration of modified-kaolinite clay particles can also be seen in Figure 6i–6k. The agglomerating domains of KAO-D clay which are highlighted in yellow circle particles may cause the reduction of tensile strength and elongation at the break of biocomposites. The high surface area and strong interfacial interactions of nanoclays with both starch and natural rubber can promote better interfacial adhesion, leading to improved blend stability.

3.6. Thermal stabilities

Due to their inherent configuration characteristics, inorganic materials exhibited greater thermal stability and thermal resistance qualities than organic ones. Hence, incorporating inorganic particles into polymers could significantly increase the thermal stability of composites consisting of natural polymers. Figure 7 depicts the thermogravimetry (TG) and derivative thermogravimetry (DTG) curves of biocomposites containing 4 wt% of MMT, KAO, and KAO-D. A preliminary weight loss was observed between 30 and 115°C . The evaporation of the water accounted for the weight loss. Three steps of decomposition were observed for biocomposites. The onset and peak temperatures were determined as shown in Table 1. Water loss occurred in the first step at temperatures below 100°C , whereas starch degradation occurred in the second step at temperatures about $270\text{--}340^\circ\text{C}$, and degradation of NR was presented in the temperature range of $360\text{--}430^\circ\text{C}$ as shown in Figure 7a. When nanoclays were mixed with SS80NR20, their decomposition temperatures increased indicating an improvement in the stability. Similar trends have been seen, with the stability improvement being ascribed to the strong interactions

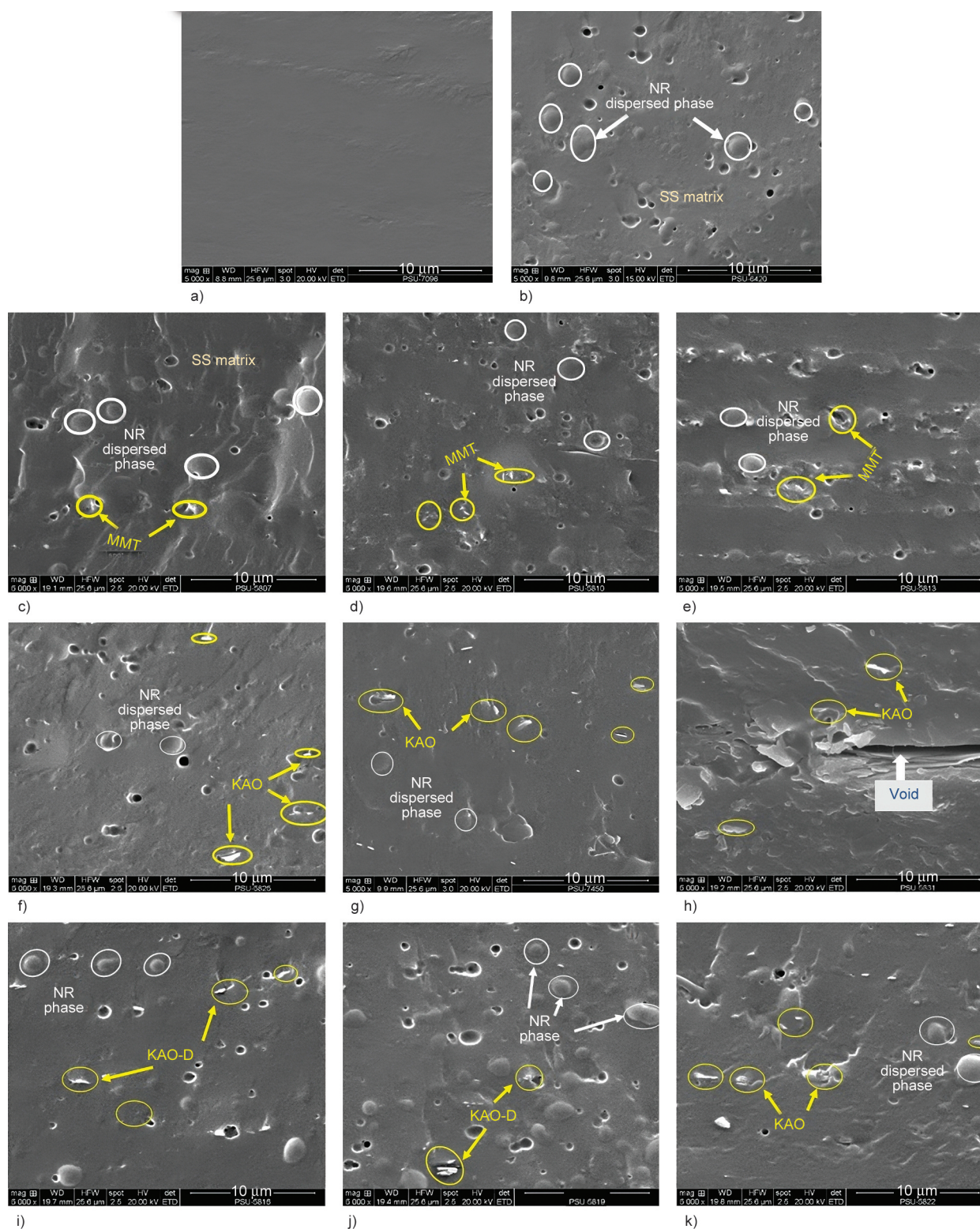


Figure 6. SEM micrographs of a) SS and b) SS80NR20 films, and biocomposites with the addition of 2, 4, and 6 wt% of c), d) e) MMT, f), g), h) KAO, and i), j), k) KAO-D.

between starch and MMT [8, 10, 32]. However, even around the temperature of 600 °C, there are some residues for all SS80NR20 blends with 9–15 wt%. These phenomena can be described that sago starch and natural rubber are polymers composed primarily of glucose and polyisoprene units, respectively. When

subjected to elevated temperatures, both starch and NR undergo thermal degradation. This degradation process involves chain scission, the release of volatile compounds, and the residual carbonaceous material. The SS80NR20 blend contains clays as inorganic materials that are not easily decomposed at the given

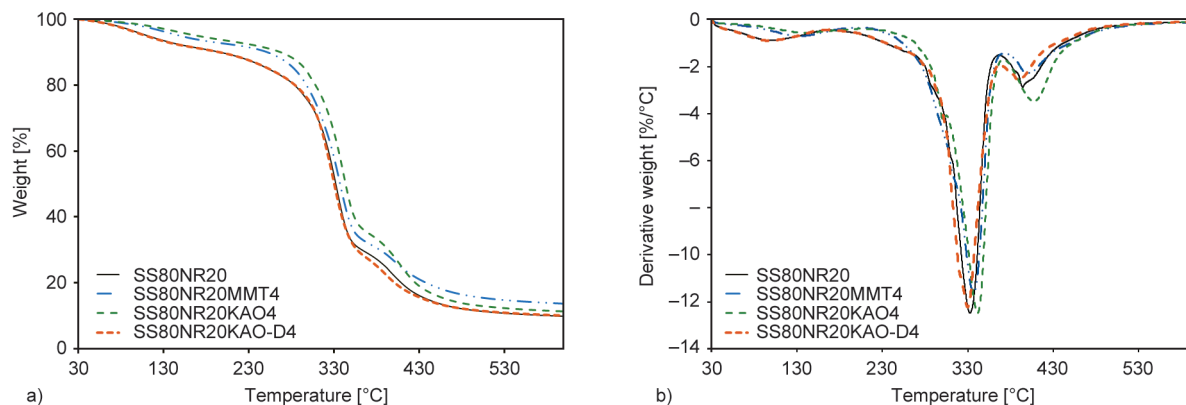


Figure 7. a) TGA and b) derivative gravimetric weight loss of biocomposites with 4 wt% of MMT, KAO, and KAO-D.

temperature range contributing to the observed residue. This improvement in the thermal stability was evident in the DTA peaks as shown in [Figure 7b](#). It is worthy of note that the thermal stability of the SS80NR20 biocomposites increased with an increase in the addition of nanoclays. The interfacial combination between NR and starch is strong when the addition of nanoclays, leads to the enhancement of thermal stability. This implies that improving the dispersion state of the nanoclay in the SS80NR20 for the intercalated nanocomposites is necessary for heat stability. The formation of a tortuous path structure in the SS80NR20 in intercalated structures could prevent or restrict the diffusion of the gases and volatile compounds produced during the decomposition. Therefore, it can be concluded that the introduction of inorganic particles would greatly improve the thermal stability of organic polymer materials [8, 32].

3.7. Dynamic mechanical investigation

DMA measures the changes in stiffness and damping by applying an oscillatory force at an established

frequency on the sample. Elastic, storage Moduli and $\tan \delta$ information were obtained using DMA data. Temperature-dependent modulus values and SS80NR20 biocomposite transitions can be observed in [Figure 8](#) which are E' and $\tan \delta$ curves. If the blends are immiscible, the $\tan \delta$ curves will indicate the presence of two damping peaks corresponding to the T_g of the different polymers [20]. If the two polymer phases are completely miscible, only one peak will be observed, which is found between the T_g of the component polymers. In SS80NR20 biocomposites with 4 wt% of kaolinite, the value of the storage modulus (E') was found to be highest at the glassy and rubbery areas, indicating that these samples were more brittle than other samples. A significant increase is noticed in T_g for all the samples compared to SS80NR20 as seen in [Table 1](#). This increases in the value of T_g is an indication of improvement in the intermolecular bonding within the SS80NR20 biocomposites. For an efficient reinforcement of S80NR20 with clays, it is crucial to a favorable interaction and a homogeneous dispersion of the

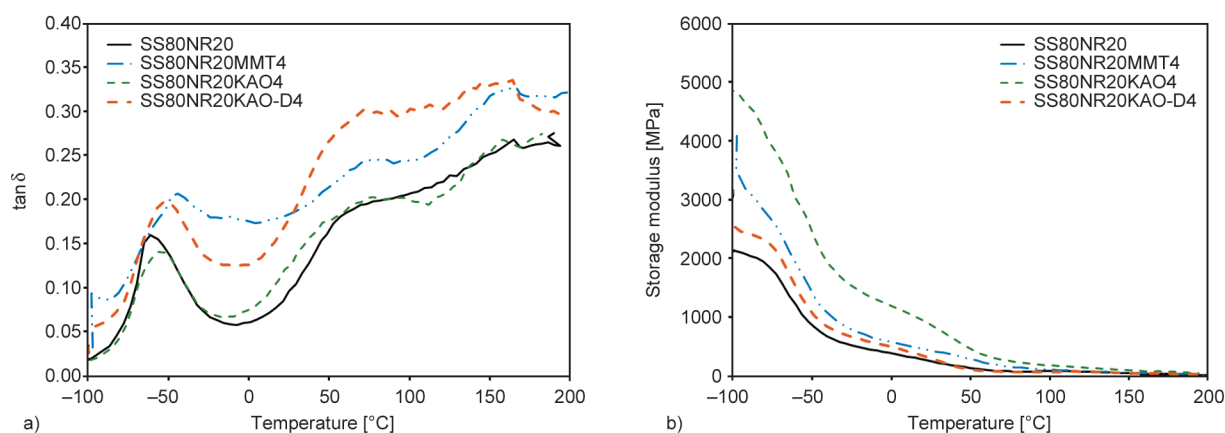


Figure 8. DMA characteristics of a) mechanical loss factor ($\tan \delta$) and b) storage modulus (E') of biocomposites with 4 wt% of clays.

Table 1. Thermal characteristics of SS80NR20 biocomposites with 4 wt% of clays.

Samples	2 nd step		3 rd step		T_g (DMA) [°C]
	T_{onset} [°C]	T_{peak} [°C]	T_{onset} [°C]	T_{peak} [°C]	
SS80NR20	222.6	333.3	362.2	394.3	-56.7
SS80NR20MMT4	253.0	337.2	371.9	404.2	-44.6
SS80NR20KAO4	266.3	341.8	371.6	408.1	-49.0
SS80NR20KAO-D4	223.0	330.8	367.9	396.4	-52.2

MMT and KAO in the SS80NR20, which will facilitate the stress transfer from the SS80NR20 to the nanoclay, increasing the rigidity of the material. $\tan \delta$ curves as a function of temperature of SS80NR20 biocomposites are shown in Figure 8b. All the samples showed three relaxation peaks in $\tan \delta$ curves. The relaxation located at lower temperatures, next to -50°C is associated with the glass transition of the NR phase, in glycerol plasticizer, while the broad relaxation that occurs at higher temperatures corresponds to the glass transition of the starch-rich phase. This contributes that when clay was present, starch and natural rubber chain mobility were more constrained [24, 32]. The SS80NR20 blends with the addition of nanoclay showed the broadening and shifting of damping peaks glass transition temperature (T_g) of NR was shifted to higher than that SS80NR20 blend which revealed some interaction between the sago starch and NR. This is related to a partially miscible blend. It was also found that, at room temperature, the stiffness of SS80NR20 is improved by the incorporation of nanoclays. These findings indicate that favorable contact and uniform dispersion of the nanoclays in the SS80NR20 blend are important for an efficient reinforcement of SS80NR20 with nanoclays. It will enable the stress transfer from the matrix to the nanoclays and increase the stiffness of the material. Comparing the types of clays, MMT helps the most improvement of the compatibility.

4. Conclusions

The following conclusions may be taken from the findings and discussion. In the blending solution process, the SS80NR20 biocomposites can be accomplished with nanoclays as reinforcing and compatibilizing fillers. The XRD characterization revealed evidence that the layered silicate is intercalated by polysaccharide and rubber chains. According to the results of XRD and SEM micrographs, it

was indicated that MMT and kaolinite clays help improve interfacial adhesion. The mechanical and physical characteristics of SS80NR20 biocomposites were attributed to the strong interaction that resulted in the intercalated structure of MMT and KAO, whereas KAO-D was accountable for the weak interaction at the SS80NR20 interface. The glass transition temperature (T_g) of the NR or SS-glycerol phase is higher than that of the SS80NR20 blend, which is another indication of the compatibilizing action of nanoclay in SS80NR20 biocomposites.

Acknowledgements

The first author gratefully acknowledges the grant support provided by the M.Sc. scholarship of Prince of Songkla University and the Scholarship Awards for graduate student.

References

- [1] Elsheekh K. M., Kamel R. R., Elsherif D. M., Shalaby A. M.: Achieving sustainable development goals from the perspective of solid waste management plans. *Journal of Engineering and Applied Science*, **68**, 9 (2021). <https://doi.org/10.1186/s44147-021-00009-9>
- [2] Moshood T. D., Nawanir G., Mahmud F., Mohamad F., Ahmad M. H., Abdulghani A.: Biodegradable plastic applications towards sustainability: A recent innovations in the green product. *Cleaner Engineering and Technology*, **6**, 100404 (2022). <https://doi.org/10.1016/j.clet.2022.100404>
- [3] Gupta V., Biswas D., Roy S.: A comprehensive review of biodegradable polymer-based films and coatings and their food packaging applications. *Materials*, **15**, 5899 (2022). <https://doi.org/10.3390/ma15175899>
- [4] Onyeaka H., Obileke K., Makaka G., Nwokolo N.: Current research and applications of starch-based biodegradable films for food packaging. *Polymers*, **14**, 1126 (2022). <https://doi.org/10.3390/polym14061126>
- [5] Mangaraj S., Yadav A., Bal L. M., Dash S. K., Mahanti N. K.: Application of biodegradable polymers in food packaging industry: A comprehensive review. *Journal of Packaging Technology and Research*, **3**, 77–96 (2019). <https://doi.org/10.1007/s41783-018-0049-y>
- [6] Chavan P., Sinhmar A., Sharma S., Dufresne A., Thory R., Kaur M., Sandhu K. S., Nehra M., Vikash N.: Nanocomposite starch films: A new approach for biodegradable packaging materials. *Starch*, **74**, 2100302 (2022). <https://doi.org/10.1002/star.202100302>
- [7] Ordoñez R., Atarés L., Chiralt V.: Biodegradable active materials containing phenolic acids for food packaging applications. *Comprehensive Review Food Science and Food Safety*, **21**, 3910–3930 (2022). <https://doi.org/10.1111/1541-4337.13011>

- [8] Romero-Bastida C. A., Tapia-Blácido D. R., Méndez-Montealvo G., Bello-Pérez L. A., Velázquez G., Alvarez-Ramirez J.: Effect of amylose content and nano-clay incorporation order in physicochemical properties of starch/montmorillonite composites. *Carbohydrate Polymers*, **152**, 351–360 (2016).
<https://doi.org/10.1016/j.carbpol.2016.07.009>
- [9] Csiszár E., Nagy A., Fekete E.: Contribution of flax-cellulose nanocrystals on the structural properties and performance of starch-based biocomposite films. *Express Polymer Letters*, **17**, 458–470 (2023).
<https://doi.org/10.3144/expresspolymlett.2023.34>
- [10] Luchese C. L., Benelli P., Spada J. C., Tessaro I. C.: Impact of the starch source on the physicochemical properties and biodegradability of different starch-based films. *Journal of Applied Polymer Science*, **135**, 46564 (2018).
<https://doi.org/10.1002/app.46564>
- [11] Behera A. K., Mohanty C., Pradhan S. K., Das N.: Assessment of soil and fungal degradability of thermoplastic starch reinforced natural fiber composite. *Journal of Polymers and the Environment*, **29**, 1031–1039 (2021).
<https://doi.org/10.1007/s10924-020-01944-z>
- [12] Müller C. M. O., Laurindo J. B., Yamashita F.: Effect of nanoclay incorporation method on mechanical and water vapor barrier properties of starch-based films. *Industrial Crops and Products*, **33**, 605–610 (2011).
<https://doi.org/10.1016/j.indcrop.2010.12.021>
- [13] Mbey J. A., Thomas F.: Components interactions controlling starch-kaolinite composite films properties. *Carbohydrate Polymers*, **117**, 739–745 (2015).
<https://doi.org/10.1016/j.carbpol.2014.10.053>
- [14] Yang J., Ching Y. C., Ching K. Y., Ran X., Al-Hada N. M., Sui X., Wei Y., Xu S., Yu J., Wang J., Zhou J.: Preparation and characterization of starch-based bioplastic films modified by citric acid-epoxidized soybean oil oligomers. *Journal of Polymers and the Environment*, **31**, 954–964 (2023).
<https://doi.org/10.1007/s10924-022-02661-5>
- [15] Ismail H., Zaaba N. F.: Tensile properties, degradation behavior, and water absorption of sago starch plastic films. *Journal of Vinyl Additive Technology*, **18**, 235–240 (2012).
<https://doi.org/10.1002/vnl.20300>
- [16] Ruamcharoen J., Munlee R., Ruamcharoen P.: Improvement of water vapor barrier and mechanical properties of sago starch-kaolinite nanocomposites. *Polymer Composites*, **41**, 201–209 (2020).
<https://doi.org/10.1002/pc.25360>
- [17] Wannaphatchaiyong S., Suksaeree J., Waiprib R., Kaewpuang A., Saelee W., Pichayakorn W.: Gelatin/gelatinized sago starch biomembranes as a drug delivery system using rubber latex as plasticizer. *Journal of Polymers and the Environment*, **27**, 2380–2394 (2019).
<https://doi.org/10.1007/s10924-019-01510-2>
- [18] Ahmad F. B., Williams P. A., Doublier J-L., Durand S., Buleon A.: Physico-chemical characterisation of sago starch. *Carbohydrate Polymers*, **38**, 361–370 (1999).
[https://doi.org/10.1016/S0144-8617\(98\)00123-4](https://doi.org/10.1016/S0144-8617(98)00123-4)
- [19] Carvalho A. J. F., Job A. E., Alves N., Curvelo A. A. S., Gandini A.: Thermoplastic starch/natural rubber blends. *Carbohydrate Polymers*, **53**, 95–99 (2003).
[https://doi.org/10.1016/S0144-8617\(03\)00005-5](https://doi.org/10.1016/S0144-8617(03)00005-5)
- [20] Rouilly A., Rigal L., Gilbert R. G.: Synthesis and properties of composites of starch and chemically modified natural rubber. *Polymer*, **45**, 7813–7820 (2004).
<https://doi.org/10.1016/j.polymer.2004.09.043>
- [21] Trovatti E., Carvalho A., Gandini A.: A new approach to blending starch with natural rubber. *Polymer International*, **64**, 605–610 (2015).
<https://doi.org/10.1002/pi.4808>
- [22] Mondragón M., Hernández E. M., Rivera-Armenta J. L., Rodríguez-González F. J.: Injection molded thermoplastic starch/natural rubber/clay nanocomposites: Morphology and mechanical properties. *Carbohydrate Polymers*, **77**, 80–86 (2009).
<https://doi.org/10.1016/j.carbpol.2008.12.008>
- [23] Ruamcharoen J., Munlee R., Ruamcharoen P.: Eco-friendly bio-based composites of cassava starch and natural rubber compatibilized with nanoclays. *Polymer Composites*, **44**, 1071–1082 (2023).
<https://doi.org/10.1002/pc.27154>
- [24] Ruamcharoen J., Ratana T., Ruamcharoen P.: Bentonite as a reinforcing and compatibilizing filler for natural rubber and polystyrene blends in latex stage. *Polymer Engineering and Science*, **54**, 1436–1443 (2014).
<https://doi.org/10.1002/pen.23665>
- [25] Katerinopoulou K., Giannakas A., Grigoriadi K., Barkoula N. M., Ladavos A.: Preparation and characterization of acetylated corn starch-(PVOH)/clay nanocomposite films. *Carbohydrate Polymer*, **102**, 216–222 (2014).
<https://doi.org/10.1016/j.carbpol.2013.11.030>
- [26] Dean K., Do M., Petinakis E., Yu L.: Key interactions in biodegradable thermoplastic starch/poly(vinyl alcohol)/montmorillonite micro- and nanocomposites. *Composites Science and Technology*, **68**, 1453–1462 (2008).
<https://doi.org/10.1016/j.compscitech.2007.10.037>
- [27] Chuayjuljit S., Worawas C.: Nanocomposites of EVA/polystyrene nanoparticles/montmorillonite. *Journal of Composite Materials*, **45**, 631–638 (2010).
<https://doi.org/10.1177/0021998310376116>
- [28] Ock H. G., Ahn K. H., Lee S. J., Hyun K.: Characterization of compatibilizing effect of organoclay in poly(lactic acid) and natural rubber blends by FT-rheology. *Macromolecules*, **49**, 2832–2842 (2016).
<https://doi.org/10.1021/acs.macromol.5b02157>
- [29] Olivato J. B., Marini J., Yamashita F., Pollet E., Grossmann M. V. E., Avérous L.: Sepiolite as a promising nanoclay for nano-biocomposites based on starch and biodegradable polyester. *Materials Science and Engineering C*, **70**, 296–302 (2017).
<https://doi.org/10.1016/j.msec.2016.08.077>

- [30] Chuayjuljit S., Wiriya-soonthorn S., Jiratumnukul N., Limpanart S.: Preparation of natural rubber/cassava starch/organomontmorillonite biodegradable nanocomposite elastomers. *Polymers and Polymer Composites*, **17**, 173–179 (2009).
<https://doi.org/10.1177/096739110901700306>
- [31] Almasi H., Ghanbarzadeh B., Entezmi A. A.: Physico-chemical properties of starch-CMC-nanoclay biodegradable films. *International Journal of Biological Macromolecules*, **46**, 1–5 (2010).
<https://doi.org/10.1016/j.ijbiomac.2009.10.001>
- [32] Derungs I., Rico M., López J., Barral L., Montero B., Bouza R.: Influence of the hydrophilicity of montmorillonite on structure and properties of thermoplastic wheat starch/montmorillonite bionanocomposites. *Polymer for Advance Technologies*, **32**, 4479–4489 (2021).
<https://doi.org/10.1002/pat.5450>